$$\frac{\alpha_2^s}{\alpha_1^s} = 1 + \frac{3(1+\epsilon_m)}{\epsilon_m} \times \frac{\left(C_{D_t}/C_{D_P}\right)(dH/A_1)\left[1-(H/L_2)+(H/L_2)e^{-L_2/H}\right]+\epsilon_m^{\frac{2}{3}}}{\left(C_{D_t}/C_{D_P}\right)(dH/A_1)+e^{-L_2/H}+\epsilon_m^{\frac{2}{3}}} \tag{14}$$

where H is the scale height, C_{D_t} and C_{D_P} are the drag coefficients for the tether and the probes, respectively, d is the tether diameter, and A_1 and A_2 are the probe frontal areas. These can be related to the mass ratio by assuming mass-volume similarity, i.e., $A_2/A_1 = \epsilon_m^{2/3}$. This relationship indicates that the most influential parameters are H/L_2 and ϵ_m. Decreasing these quantities increases the pitch angle ratio. Generally, the dynamic response is due to the combined influence of the drag and the eccentricity. The drag-perturbed differential equations were linearized and solved by the WKBJ method. The conclusion is that, although the drag alters the dynamics by adding new even-periodic terms, a small drag causes a bounded motion with no resonance.

The influence of the drag can be observed by plotting the bifurcation of the angles with the eccentricity as the bifurcation parameter (Fig. 1). These plots are a stroboscopic sampling of the phase plane at each perigee passage. The initial conditions are zero so that the plots describe the eccentricity excitation for a variety of eccentricities. The atmospheric drag breaks the pitch symmetry (which can be inferred from the structure of the differential equations) and alters the periodic solution. A possible explanation for the amplification of the drag effect at low eccentricity is its noncommensurability with the eccentricity excitation. Also, because the perigee altitude is kept constant, the average drag varies as $(1-e)$ and, consequently, a circular orbit has the highest drag effect. A penetration down to altitudes less than $H_p = 130$ km without any tether control system appears feasible for a single-probe tethered system, whereas the stability of the lowest probe in a dual-probe system is more marginal. Figure 2 shows the roles of ϵ_m and ϵ_L within the attitude dynamics of the system with and without drag. Increasing ϵ_L increases the amplitudes of the pitch motion, whereas ϵ_m plays the opposite role in the perturbed and unperturbed dynamics.

IV. Concluding Remarks

The dual-probe configuration examined in this Note seems suitable for reaching altitudes as low as 130 km in the Earth's atmosphere. A single-probe tether system is preferable for reaching even lower altitudes. The dynamic behavior of the dual-probe system is characterized by a typical amplitude ratio of 4:1 between the pitch angles of the lower and upper probes. This ratio becomes larger at low altitudes when the upper tether performs small librations and the lower probe oscillates more strongly. The eccentricity excitation results in bounded oscillations for small eccentricities. A small length ratio is preferable, especially at low altitudes, because the drag acting on the lower tether induces large pitch oscillations on the lowest probe. The analytical results are comparable with numerical simulations of the equations of motion. The release of some simplifying assumptions by including, for example, tether flexibility and elasticity, has small effects for small librations and tethers of suitable stiffness.[2]

References

[1]Lorenzini, E. C., Cosmo, M. L., Grossi, M. D., Chance, K., and Davis, J. C., "Tethered Multi-Probe for Thermospheric Research," *Proceedings of the Fourth International Conference on Tethers in Space* (Washington, DC), Science and Technology Corp., Hampton, VA, 1995, pp. 1567–1576.

[2]Beletsky, V. V., and Levin, E. M., *Dynamics of Space Tether System, Advances in the Astronautical Sciences*, Vol. 83, American Astronautical Society, San Diego, CA, 1993, pp. 20–33.

[3]Misra, A. K., and Modi, V. J., "A Survey of the Dynamics and Control of Tethered Satellite Systems," *Advances in the Astronautical Sciences, Tethers in Space*, Vol. 62, 1986, pp. 667–719.

[4]Misra, A. K., Amier, Z., and Modi, V. J., "Attitude Dynamics of Three-Body Tethered System," *Acta Astronautica*, Vol. 17, No. 10, 1988, pp. 1059–1068.

[5]Cunningham, W. J., *Introduction to Nonlinear Analysis*, McGraw–Hill, New York, 1958, pp. 253–257.

[6]Modi, V. J., and Brereton, R. C., "Libration Analysis of a Dumbbell Satellite Using the WKBJ Method," *Journal of Applied Mechanics*, Vol. 33, No. 3, 1966, pp. 676–678.

[7]Nayfeh, A. H., and Mook, D. T., *Nonlinear Oscillations*, Wiley-Interscience, New York, 1979, p. 556.

Dynamical Characteristics of a Tethered Stabilized Satellite

Joshua Ashenberg* and Enrico C. Lorenzini†
Harvard–Smithsonian Center for Astrophysics, Cambridge, Massachusetts 02138

Nomenclature

A	= tether cross-section area
E	= tether material Young's modulus
f	= orbit true anomaly
L	= tether length
M	= satellite mass
m	= ballast mass
$\boldsymbol{r}$	= satellite orbit radius vector
T	= tether tension
$\alpha_1, \alpha_2, \alpha_3$	= satellite roll, pitch, and yaw angles
δ_1, δ_2	= roll and pitch control angles
θ_1, θ_2	= tether roll and pitch angles
μ	= gravitational constant
ρ	= offset of attachment point with respect to satellite center of mass
ρ_m	= tether material density
Ω	= orbital angular velocity
ω	= satellite angular velocity

I. Introduction

THE restoring torque of a gravity gradient-stabilized satellite can be enhanced significantly by adding a tether.[1] A possible way to stabilize an Earth-pointing satellite is by attaching the tether, with a ballast at its opposite end, to the leeward side of the satellite. A further improvement can be obtained by moving the attachment point over a two-dimensional surface.[2] This modification changes the stabilization method from passive to active. This concept may be very attractive for satellites with moderate-to-high pointing accuracy requirements that could be achieved by means of a low-energy controller.

This work presents a preliminary investigation of the stability characteristics of a tethered satellite attitude with respect to the local vertical. Other relevant topics analyzed are the influence of orbital eccentricity and tether oscillations on the satellite dynamics and identification of possible resonances. Parameters that affect the attitude control are the tether length, the offset between the satellite center of mass and the attachment point, and the ballast mass. The configuration under investigation consists of a satellite, a tether, and a ballast mass at the opposite end of the tether. The position of the movable tether attachment point is controlled by the stabilization control logic. To separate the tether dynamics from the satellite dynamics, we assume realistically that $\rho \ll L$ (typically $\rho < 1m$

Received Aug. 8, 1996; revision received April 23, 1997; accepted for publication June 23, 1997.

*Consultant, Radio and Geoastronomy Division, Mail Stop 80. Member AIAA.

†Staff Scientist, Radio and Geoastronomy Division, Mail Stop 80. Senior Member AIAA.

and $L > 100m$). Note that, although the attitude dynamics of a small satellite does not affect significantly the libration dynamics of a long tether, the opposite is not true. Also, we adopt small ballast masses, typically 1% of the satellite mass, to prove that a light stabilization system is sufficient. The satellite follows an unperturbed Keplerian orbit so that only the tether librations are excited. The satellite principal body frame is rotated from the LV–LH (local vertical–local horizontal) orbital frame by the sequence $\alpha_3 \to \alpha_2 \to \alpha_1$ or yaw–pitch–roll, respectively. The offset control vector $\boldsymbol{\rho}$ can rotate by the pitch (δ_2) and the roll angle (δ_1) with respect to the principal body frame. The tether reference frame is identified by the pitch rotation (θ_2) and roll rotation (θ_1) with respect to the LV–LH frame.

The general form of the satellite equations of motion is

$$\boldsymbol{I}\cdot\frac{\mathrm{d}}{\mathrm{d}t}\boldsymbol{\omega}+\boldsymbol{\omega}\times\boldsymbol{I}\cdot\boldsymbol{\omega}=3\frac{\mu}{\boldsymbol{r}^3}\hat{\boldsymbol{r}}\times\boldsymbol{I}\cdot\hat{\boldsymbol{r}}+\boldsymbol{\rho}\times\boldsymbol{T} \tag{1}$$

where the right-hand terms represent the gravity gradient and tension control. After defining K_j as the inertia ratios

$$K_1=\frac{I_2-I_3}{I_1},\qquad K_2=\frac{I_1-I_3}{I_2},\qquad K_3=\frac{I_2-I_1}{I_3} \tag{2}$$

and $\lambda_j=(\bar{m}L\rho/I_j)$ as the stiffness control parameter, linearizing the equations of motion, and expressing the equations in terms of the true anomaly f, the linearized equations for small eccentricity orbits become

$$\begin{aligned}
&(1+e\cos f)\alpha_1''-2e\sin f\alpha_1'-(1-K_1)(1+e\cos f)\alpha_3'\\
&\quad+[(4+e\cos f)K_1+(3+e\cos f)\lambda_1]\alpha_1\\
&\quad=\lambda_1(3+e\cos f)(\theta_1-\delta_1)\\
&(1+e\cos f)\alpha_2''-2e\sin f\alpha_2'+3\Big[K_2+\Big(1+\tfrac{1}{3}e\cos f\Big)\lambda_2\Big]\alpha_2\\
&\quad=-2e\sin f+\lambda_2(3+e\cos f)(\theta_2-\delta_2)\\
&(1+e\cos f)\alpha_3''-2e\sin f\alpha_3'+(1-K_3)(1+e\cos f)\alpha_1'\\
&\quad+K_3(1+e\cos f)\alpha_3=0
\end{aligned} \tag{3}$$

Note that a circular orbit ($e=0$) would be preferable for an Earth-pointing satellite because the eccentricity excites tether librations that in turn affect the satellite attitude dynamics. Inspection of Eq. (3) shows that λ_j plays the role of an additional attitude restoring torque, i.e., increased stiffness, and a multiplier of the control torque. Considering that λ_j is much greater than 1 (typically in the hundreds), the natural modes and the stability of a tethered stabilized satellite are quite different from that of a nontethered (or free) satellite. The following analysis clarifies this issue.

II. Stability Analysis

Linearization of the motion equations decouples the pitch from the roll–yaw dynamics. This is true even for large-pitch oscillations and small roll–yaw oscillations. However, the roll–yaw response may resonate with the nonlinear pitch.[3] The eccentricity excites the satellite attitude through two mechanisms: a direct effect as a result of orbit ellipticity and an indirect effect because of tether excitation. The tether pitch libration (in the orbital plane) forced by the orbital eccentricity is described by the following equation[4]:

$$\theta_2=e\Big[\sin f-\Big(1/\sqrt{3}\Big)\sin\sqrt{3}f\Big] \tag{4}$$

Substituting into the pitch equation and changing variables,[5] $\alpha_2=\beta/(1+e\cos f)$, results in the following nonhomogeneous equation:

$$\begin{aligned}
&\beta''+\frac{e\cos f+3\Big[K_2+\Big(1+\frac{1}{3}e\cos f\Big)\lambda_2\Big]}{1+e\cos f}\beta\\
&\quad=-2e\sin f+\lambda_2 e\,(3+e\cos f)\left(\sin f-\frac{1}{\sqrt{3}}\sin f\right)
\end{aligned} \tag{5}$$

Unlike for a free satellite, there are no periodic solutions of Eq. (5). This is because of the noncommensurability of the tether libration frequencies.

First, possible resonances are identified. The expansion of the differential equation in terms of small eccentricity

$$\beta''+\Big(G_0^2+eG_1^2+e^2G_2^2+\text{H.O.T.}\Big)\beta=eF_0+e^2F_1 \tag{6}$$

where $G_0^2=3(K_2+\lambda_2)$, and the following are more involved functions in the form $G_j=G_j(K_2,\lambda_2;f)$ $F_j=F_j(K_2,\lambda_2;f)$. Expanding β as

$$\beta=\beta_0+e\beta_1+e^2\beta_2+\text{H.O.T.} \tag{7}$$

results in the following set of equations:

$$\begin{aligned}
&e^0\colon \beta_0''+G_0^2\beta_0=0,\qquad e^1\colon \beta_1''+G_0^2\beta_1=F_0-G_1^2\beta_0\\
&e^2\colon \beta_2''+G_0^2\beta_2=F_1-G_1^2\beta_1-G_2^2\beta_0
\end{aligned} \tag{8}$$

The particular solutions of these equations indicate resonant conditions for the order e and e^2, as follows:

$$\begin{aligned}
&O(e)\colon K_2+\lambda_2=\Big\{\tfrac{1}{3},1\Big\}\\
&O(e^2)\colon K_1+\lambda_2=\Big\{\tfrac{1}{3}(\sqrt{3}-1)^2,\tfrac{4}{3},\tfrac{1}{3}(\sqrt{3}+1)^2\Big\}
\end{aligned} \tag{9}$$

Unlike a free satellite, realistic configurations of tethered satellites are outside the resonant region. Higher-order resonances correspond to higher values of λ_2 but have negligible magnitudes of order $O(e^k)$.

In the following, the eccentricity-excited solution for a configuration with a large λ is derived. The approximate equation of motion for $e\ll 1$ and $\lambda_2\gg 1$ is

$$\begin{aligned}
&\beta''+3\Big[K_2+\Big(1-\tfrac{2}{3}e\cos f\Big)\lambda_2\Big]\beta\\
&\quad\approx 3\lambda_2 e\Big[\sin f-\Big(1/\sqrt{3}\Big)\sin\sqrt{3}f\Big]
\end{aligned} \tag{10}$$

This differential equation is solved by applying the WKBJ method.[4] Because it can be shown that the error as a result of the approximations is of order $O[e/(K_2+\lambda_2)^2]$, the results obtained for a tethered satellite are more accurate than the results obtained from Eq. (10) for a free satellite because $\lambda_2\gg K_2$. The resulting particular solution is

$$\begin{aligned}
\beta=e\frac{\lambda_2}{K_2+\lambda_2-\frac{1}{3}}\Bigg[&\sin f+\frac{1}{\sqrt{3(K_2+\lambda_2)}}\left(\frac{K_2+\lambda_2-\frac{1}{3}}{K_2+\lambda_2-1}-1\right)\\
&\times\sin\sqrt{3(K_2+\lambda_2)}f-\frac{1}{\sqrt{3}}\frac{K_2+\lambda_2-\frac{1}{3}}{K_2+\lambda_2-1}\sin\sqrt{3}f\Bigg]
\end{aligned} \tag{11}$$

Note that the amplitude related to the natural frequency $\{\sqrt{[3(K_2+\lambda_2)]}\}$ is of order $O[(1/\lambda_2^{3/2})]$ relative to the amplitude related to the forcing frequencies $(1,\sqrt{3})$. Consequently, for a large value of λ_2,

$$\beta_{\lambda_2\gg 1}\approx e\Big[\sin f-\Big(1/\sqrt{3}\Big)\sin\sqrt{3}f\Big] \tag{12}$$

that is, for large values of the stiffness control parameter, the satellite and the tether oscillate as a single rigid body.

The decoupling of the pitch and the roll–yaw dynamics enable us to investigate the three-axis stability of the tethered satellite in a way that is analogous to the classic gravity gradient stabilization[6] analysis of (nontethered) satellites. The three-axis dynamics in a circular orbit is expressed by the following equations:

$$\begin{aligned}
&\ddot{\alpha}_2+3\Omega^2(K_2+\lambda_2)\alpha_2=0\\
&\begin{pmatrix}\ddot{\alpha}_1\\ \ddot{\alpha}_3\end{pmatrix}+\boldsymbol{G}\begin{pmatrix}\dot{\alpha}_1\\ \dot{\alpha}_3\end{pmatrix}+\boldsymbol{K}\begin{pmatrix}\alpha_1\\ \alpha_3\end{pmatrix}=0
\end{aligned} \tag{13}$$

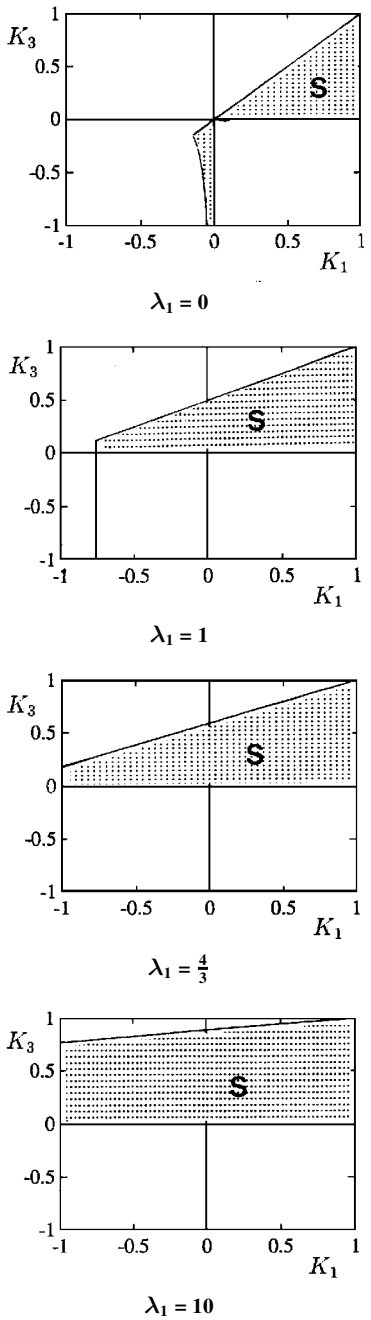

Fig. 1 Three-axis stability diagram.

where $\boldsymbol{G}$ is a gyric matrix

$$\boldsymbol{G} = \Omega\begin{bmatrix} 0 & -(1-K_1) \\ (1-K_3) & 0 \end{bmatrix} \tag{14}$$

and $\boldsymbol{K}$ is a stiffness matrix

$$\boldsymbol{K} = \Omega^2\begin{bmatrix} 4\left(K_1 + \frac{3}{4}\lambda_1\right) & 0 \\ 0 & K_3 \end{bmatrix} \tag{15}$$

The condition for pitch stability is $K_2 + \lambda_2 > 0$, which corresponds, in the $K_1 - K_3$ plane, to $K_3 < [1/(1+\lambda_1)](K_1 + \lambda_1)$. The main point of this result is that for a tethered satellite I_1 does not necessarily need to be greater than I_3, as in the case of a free satellite. It is shown in Fig. 1 that most of the $K_1 - K_3$ region is permitted for pitch stability. The only exception is a triangular area, mostly where $I_3 > I_2 > I_1$, that narrows as λ_1 increases.

The roll–yaw stability is determined by the gyric and stiffness matrices. Because the system under analysis is a conservative gyric system, a sufficient condition for stability is $\boldsymbol{K} > 0$, i.e., static stability. This condition implies $K_3 > 0$ and $K_1 > -\frac{3}{4}\lambda_1$. When $\lambda_1 \geq \frac{4}{3}$, the system is stable in the entire upper half of the $K_1 - K_3$ plane. The characteristic polynomial for the roll–yaw stability is

$$s^4 + s^2(\mathrm{tr}\,\boldsymbol{K} + \det\boldsymbol{G}) + \det\boldsymbol{K} = 0 \tag{16}$$

The system is marginally stable if $\det\boldsymbol{K} > 0$ and $(\mathrm{tr}\,\boldsymbol{K} + \det\boldsymbol{G})^2 > 4\det\boldsymbol{K}$. The former condition gives two possibilities: 1) $K_3 > 0$ and $K_1 > -\frac{3}{4}\lambda_1$, i.e., static stability for $\boldsymbol{K}$ positive definite; and 2) $K_3 < 0$ and $K_1 < -\frac{3}{4}\lambda_1$, i.e., gyric stability for $\boldsymbol{K}$ negative definite. The latter condition can be expressed a s $(1 + 3K_1 + K_1K_3 + 3\lambda_1)^2 - 16K_3(K_1 + \frac{3}{4}\lambda_1) > 0$. The role of the stiffness and gyric contributions is simple. The tether tension dominates one of the stiffness matrix eigenvalues but does not influence the gyric matrix. Therefore, large values of the tether tension strengthen the negative definite nature of $\boldsymbol{K}$ for $I_1 > I_2$. The gyric stabilization is insufficient to overcome the static destabilization. The three-axis stability is shown by the shaded area in Fig. 1.

Next we consider the influence of the tether flexible modes, whose frequencies are typically in tens up to hundreds of cycles per orbit. The purpose of the following analysis is to identify possible resonances. Assuming small amplitude librations in a circular orbit, we first investigate the pitch response of the satellite. After modeling the oscillating tension as

$$\lambda_2 = \lambda_2^0(1 + \epsilon\cos\omega f) \tag{17}$$

substituting into the pitch equation and changing the independent variable as $\tau = \omega f$, the pitch response is described by a 2π-period Hill's equation

$$\frac{\mathrm{d}^2\alpha_2}{\mathrm{d}\tau^2} + \frac{3\lambda_2^0}{\omega^2}\left(1 + \frac{K_2}{\lambda_2^0} + \epsilon\cos\tau\right)\alpha_2 = 0 \tag{18}$$

A parametric resonance for $\epsilon \to 0$ occurs for the following condition:

$$\lambda_2^0 + K_2 = (\omega^2/12)k^2, \qquad k = 1, 2, \ldots \tag{19}$$

Because the tongues of unstable motion (see Fig. 2) in the $\epsilon - \lambda^0$ diagram become narrower as ϵ^k, only $k = 1, 2$ are considered here. The lowest longitudinal frequency[7] (per orbit) is $\omega_{L_1} \approx (1/\Omega)\sqrt{(EA/mL)}$. The lowest transverse frequency[7] is $\omega_{T_1} \approx \pi\sqrt{(3m/\rho_m AL)}$. The next transverse frequency is $\omega_{T_2} = 2\omega_{T_1}$. Substituting λ^0 and eliminating L gives the resonant length due to either longitudinal or transverse tether oscillations, respectively,

$$L \approx \frac{1}{\Omega}\sqrt{\frac{EAI_2}{12m^2\rho}} \quad \text{or} \quad L \approx \frac{\pi}{2}\sqrt{\frac{I_2}{\rho_m A\rho}} \tag{20}$$

A similar argument leads to the conditions for parametric resonance in the roll response

$$\lambda_1^0 + \tfrac{4}{3}K_1 = (\omega^2/12)k^2, \qquad k = 1, 2, \ldots \tag{21}$$

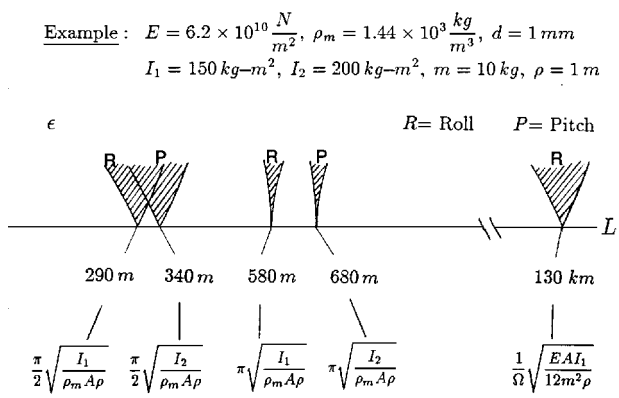

Fig. 2 Parametric resonance in pitch–roll.

Because of the three-axis stability requirement, I_2 must be greater than I_1, which is equivalent to $\lambda_1^0 > \lambda_2^0$. Consequently, the resonant lengths for the roll motion are shorter than the resonant lengths for the pitch motion. The results, shown in Fig. 2, are summarized in the following inequalities:

$$L < \frac{\pi}{2}\sqrt{\frac{I_1}{\rho_m A \rho}}, \qquad \frac{\pi}{2}\sqrt{\frac{I_2}{\rho_m A \rho}} < L < \pi\sqrt{\frac{I_1}{\rho_m A \rho}}$$
$$\pi\sqrt{\frac{I_2}{\rho_m A \rho}} < L < \frac{1}{\Omega}\sqrt{\frac{EAI_1}{12m^2\rho}} \tag{22}$$

Referring to Fig. 2, tether lengths $L < 250m$ and $L > 1km$ are safe because they are clear of unmodeled frequencies. Another interesting point is that the pitch and the roll stiffness are equal when $4K_1 + 3\lambda_1 = 3K_2 + 3\lambda_2$. In case of large stiffness control parameters, this equality implies $\lambda_1 = \lambda_2$ or $I_1 = I_2$. This condition must be avoided to prevent a possible nonlinear resonance in pitch–roll. The general condition $k(4K_1 + 3\lambda_1) = l(3K_2 + 3\lambda_2)$, for integers k and l, may also lead to natural resonances. A tethered gravity-gradient satellite is free of this problem because the frequencies $\sqrt{3}$ and 2 are well separated and are noncommensurate.

III. Concluding Remarks

The passive attitude stabilization by means of a tether appears promising for Earth-pointing satellites with moderate-to-high pointing accuracies. The preliminary investigation presented in this Note points out the following main results.

The control/restoring torque is strong enough for the pitch–roll responses. A linear controller cannot provide a direct yaw control torque. The yaw control may be designed by using the linear or the nonlinear coupling or by installing a reaction wheel if a better yaw response is required. The pitch is very stable, even for configurations with $I_3 > I_2 > I_1$, as opposed to a nontethered gravity-gradient stabilized satellite. The three-axis stability region covers most of the plane $I_2 > I_1$. The DeBra–Delp gyric stability disappears. Moreover, there is a tradeoff to be made between stability and disturbance rejection when the tether length is selected. Although a long tether provides large restoring torque, a short tether is better for filtering out high frequencies. A long tether makes the system very stiff and sensitive to external disturbances. The pointing accuracy may be better for a longer tether in an unperturbed circular orbit, but unavoidable environmental perturbations acting on the tether will be transmitted to the satellite and affect its pointing accuracy. Typical satellite-tether configurations are outside the orbital eccentricity resonance region. However, parametric resonances as a result of interaction between the satellite and the tether flexible modes may occur for some configurations and must be examined carefully for each design.

References

[1]Beletsky, V. V., and Levin, E. M., *Dynamics of Space Tether System, Advances in the Astronautical Sciences*, Vol. 83, American Astronautical Society, San Diego, CA, 1993.

[2]Lemke, L. G., Powell, J. D., and He, X., "Attitude Control of Tethered Spacecraft," *Journal of the Astronautical Sciences*, Vol. 35, No. 1, 1987, pp. 41–55.

[3]Kane, T. R., "Attitude Stability of Earth-Pointing Satellites," *AIAA Journal*, Vol. 3, No. 4, 1964, pp. 726–731.

[4]Modi, V. J., and Brereton, R. C., "Libration Analysis of a Dumbbell Satellite Using the WKBJ Method," *Journal of Applied Mechanics*, Vol. 33, No. 3, 1966, pp. 676–678.

[5]Hayashi, C., *Nonlinear Oscillations in Physical Systems*, Princeton Univ. Press, Princeton, NJ, 1985.

[6]DeBra, D. B., and Delb, R. H., "Rigid Body Attitude Stability and Natural Frequencies in a Circular Orbit," *Journal of the Astronautical Sciences*, Vol. 8, No. 1, 1961, pp. 14–17.

[7]Misra, A. K., and Modi, V. J., "A Survey on the Dynamics and Control of Tethered Satellite Systems," *Dynamics of Space Tether System, Advances in the Astronautical Sciences*, Vol. 62, American Astronautical Society, San Diego, CA, 1986, pp. 667–719.

Aircraft Trajectory Optimization in the Horizontal Plane

Valery I. Heymann*
Israel Aircraft Industries, Inc., Yehud 56000, Israel
and
Joseph Z. Ben-Asher†
Tel-Aviv University, Tel-Aviv 69978, Israel

I. Introduction

OPTIMIZATION of atmospheric flight trajectories has been of great interest for many decades. Time-optimal trajectories in the horizontal plane have been investigated either with soft control constraints,[1,2] via a quadratic penalty in the cost, or with hard constraints,[3–5] i.e., with strictly bounded control functions. The prevailing optimization method has been the minimum principle.

This work considers the planar time-optimal trajectory problem with hard control constraints and under the assumption of constant aircraft velocity, which simplifies the problem considerably.[4] The case with no wind is investigated thoroughly in Ref. 3, where it is shown that the optimal trajectories are composed of bang, i.e., maximum turn rate, and singular, i.e., level flights with zero turn rate, segments with a maximum number of four turns. Shapira and Ben-Asher[5] proposed the problem of introducing winds into the formulation. Unfortunately, closed-form expressions have not been obtained in the presence of winds, even for the restricted bang–singular–bang trajectories[5] (a simple case recommended in Ref. 3 for practical applications).

The main objective of the present research is to develop an optimization technique to obtain planar time-optimal trajectories in the presence of winds. As opposed to all previous publications on this topic, the approach taken is not based on the minimum principle. Instead, it employs a parameterization technique, originally developed for a class of bilinear systems,[6] which fits nicely to the problem of interest. The technique transforms the problem into a finite dimensional optimization problem.

The problem is formulated in Sec. II. Section III analyzes the problem and makes the mentioned transformation to the finite dimensional space. Finally, representative numerical results that manifest the nature of the solution are given in Sec. IV, and the conclusions are drawn in Sec. V.

II. Problem Formulation

Assuming constant velocity (more precisely, constant true air speed) and constant altitude, the aircraft equations of motion in the horizontal plane can be written as

$$\dot{x}(t) = V\cos[\sigma(t)] + W_x(t)$$
$$\dot{y}(t) = V\sin[\sigma(t)] + W_y(t), \qquad \dot{\sigma}(t) = u(t) \tag{1}$$

where $x(t)$ and $y(t)$ are displacements with respect to the ground, V is the true air speed, and $W_x(t)$ and $W_y(t)$ are components of the wind velocity. No position dependence, i.e., homogeneous wind field, is assumed; $\sigma(t)$ is the heading angle of the aircraft; and $u(t)$ is the control variable. We assume that $u(t)$ is constrained by $u(t) \in [-b, b]$.

The optimization problem is to find the control time history, which drives the system (1) from a given initial condition $\{x(0) = x_0, y(0) = y_0, \sigma(0) = 0\}$ to a required target point $\{x(T) = x_T, y(T) = y_T, \sigma(T) = \sigma_T \geq 0\}$ while minimizing the transition time T.

Received Dec. 2, 1996; revision received July 24, 1997; accepted for publication July 30, 1997.

*Research Engineer, MBT Division.

†Adjunct Professor, Department of Electrical Engineering—Systems. Member AIAA.